

# Evolution of the mass function of dark matter haloes

Darren Reed,<sup>1★</sup> Jeffrey Gardner,<sup>2</sup> Thomas Quinn,<sup>1</sup> Joachim Stadel,<sup>3</sup>  
Mark Fardal,<sup>4</sup> George Lake<sup>1</sup> and Fabio Governato<sup>1,5</sup>

<sup>1</sup>*Astronomy Department, University of Washington, Seattle, WA 98195, USA*

<sup>2</sup>*Physics and Astronomy Department, University of Pittsburgh, 3941 O'Hara Street, Pittsburgh PA 15 260, USA*

<sup>3</sup>*Institute for Theoretical Physics, University of Zurich, Winterthurerstrasse 190, CH-8057 Zurich, Switzerland*

<sup>4</sup>*Physics and Astronomy Department, University of Victoria, Victoria, BC, V8P 1A1, Canada*

<sup>5</sup>*Osservatorio Astronomico di Brera, via Brera 28, 20121, Milano, Italy*

Accepted 2003 August 11. Received 2003 August 8; in original form 2003 January 13

## ABSTRACT

We use a high-resolution  $\Lambda$ CDM numerical simulation to calculate the mass function of dark matter haloes down to the scale of dwarf galaxies, back to a redshift of 15, in a  $50 h^{-1}$  Mpc volume containing 80 million particles. Our low-redshift results allow us to probe low- $\sigma$  density fluctuations significantly beyond the range of previous cosmological simulations. The Sheth & Tormen mass function provides an excellent match to all of our data except for redshifts of 10 and higher, where it overpredicts halo numbers increasingly with redshift, reaching roughly 50 per cent for the  $10^{10}$ – $10^{11} M_{\odot}$  haloes sampled at redshift 15. Our results confirm previous findings that the simulated halo mass function can be described solely by the variance of the mass distribution, and thus has no explicit redshift dependence. We provide an empirical fit to our data that corrects for the overprediction of extremely rare objects by the Sheth & Tormen mass function. This overprediction has implications for studies that use the number densities of similarly rare objects as cosmological probes. For example, the number density of high-redshift ( $z \simeq 6$ ) QSOs, which are thought to be hosted by haloes at  $5\sigma$  peaks in the fluctuation field, are likely to be overpredicted by at least a factor of 50 per cent. We test the sensitivity of our results to force accuracy, starting redshift and halo-finding algorithm.

**Key words:** galaxies: clusters: general – galaxies: formation – galaxies: haloes – cosmology: theory – dark matter.

## 1 INTRODUCTION

Cold dark matter models with a cosmological constant ( $\Lambda$ CDM) are successful in explaining a wide array of kinematic and structural properties of the observed universe. A critical test of the  $\Lambda$ CDM model is how well it predicts the abundance of dark matter haloes, which serve as hosts for observable clusters, groups, and galaxies. Simulations that resolve haloes out to high redshift can be used to model the evolution of the numbers of observable high-redshift objects, their progenitors, and their evolved descendants. Lyman-break galaxies, for example, observed at redshifts out to  $z \simeq 4$  (e.g. Steidel et al. 1996) are likely progenitors of groups or clusters (Governato et al. 1998, 2001), and we are able to model their numbers over their entire observable lifespan. Many objects, however, lie outside the realm that can presently be simulated because their number densities, masses, or redshifts are too extreme. For example, to model a reasonably sized sample of the hosts of the highest redshift ( $z \simeq$

6) quasi-stellar objects (QSOs), the number density of which has been measured by the Sloan Digital Sky Survey (Fan et al. 2001), would require a simulation with volume roughly as large as the observable universe with (so far) prohibitively high particle numbers. Simulations of adequate resolution and volume could be used, in principle, to estimate the host masses of such rare QSOs, or to estimate cosmological parameters after assuming host masses, by matching predicted and observed number densities. However, with much less computational effort, by modelling smaller cosmological volumes at higher redshift, we are able to test analytic mass functions in the same regime of rare density enhancements. Generally, rare density peaks correspond to high values of  $M/M_*$ , where  $M_*$  is the ‘characteristic’ mass of a typical collapsing halo at that epoch (to be discussed later). By modelling haloes over a wide range of  $M/M_*$ , we can constrain analytic mass functions for ranges of redshift and mass that have not yet been simulated. This is possible because analytic mass functions are generally derived from assumptions of how linear density fluctuations lead to halo collapse, and thereby have no explicit redshift dependence. High-redshift QSO hosts, galaxy progenitors, and perhaps even the first generation of

★E-mail: reed@astro.washington.edu

stars are all examples of high  $M/M_*$  objects with mass functions that can presently only be calculated analytically.

Press & Schechter (P-S, 1974) developed an analytical framework that predicts the number and formation epoch of dark matter haloes. In P-S theory, as the universe evolves, linear density fluctuations grow gravitationally until they reach a critical spherical overdensity, at which time non-linear gravitational collapse is assumed to occur. Cosmological numerical simulations have shown the P-S framework to be approximately correct, but P-S theory consistently underpredicts the number of high-mass haloes and overestimates the number of haloes less than about  $M_*$  (e.g. Efstathiou et al. 1988; Gross et al. 1998; Governato et al. 1999; Jenkins et al. 2001; White 2002) even when merging of dark matter haloes is included in predictions (Bond et al. 1991; Bower 1991; Lacey & Cole 1993; Gardner 2001), though the high-mass end fits well if the finite size of haloes is taken into account (Yano, Nagashima & Gouda 1996; Nagashima 2001). Ellipsoidal halo collapse models (e.g. Monaco 1997a,b; Lee & Shandarin 1998; Sheth, Mo & Tormen 2001) yield much more robust predictions than the conventional spherical collapse models, and are in excellent agreement with empirical fits by Sheth & Tormen (1999). Monaco et al. (2002), using the semi-analytic code PINOCCHIO, which uses a perturbative approach, show that the dark matter halo distribution can be accurately predicted at much lower computational cost, on a point-by-point basis, from a numerical realization of an initial density field. Jenkins et al. (2001) utilize a large set of simulations of a range of volumes and cosmologies (Jenkins et al. 1998; Governato et al. 1999; Evrard et al. 2002) to test the Sheth & Tormen (S-T) mass function over more than four orders of magnitude in mass, and out to a redshift of 5, finding good agreement with the S-T function down to their resolution limit of  $\simeq 3 \times 10^{11} M_\odot$ , except for an overprediction by the S-T function for haloes at rare density enhancements. In this study, we probe previously untested regimes of the mass function by simulating a volume that resolves haloes down to the scale of  $10^{10} M_\odot$  dwarfs, in a cosmological environment, allowing us to sample the mass function back to  $z \simeq 15$ . Our paper is outlined as follows: in Section 2, we describe our simulations and numerical techniques; in Section 3, we review the analytic theory; we then discuss our results and compare with previous work in Section 4; we conclude with a discussion of the implications of our work.

## 2 THE SIMULATIONS

Our cosmology is the presently favoured  $\Lambda$ CDM with  $\Lambda = 0.7$  and  $\Omega_m = 0.3$ . We use the parallel tree gravity solver PKDGRAV (Stadel 2001) to simulate  $81 \times 10^6$  ( $432^3$ ) dark matter particles from a starting redshift,  $z_0$ , of 69. We then resimulate the same volume but with  $z_0 = 139$ , and evolve this volume to  $z = 7$ , which allows us to consider results at higher redshift than with the  $z_0 = 69$  run. In order to simulate the highest possible mass resolution, we employ a volume of  $50 h^{-1}$  Mpc on a side. Our particle mass is

$1.3 \times 10^8 h^{-1} M_\odot$  allowing us to resolve haloes down to less than  $10^{10} h^{-1} M_\odot$  with 75 particles. Our force resolution is  $5 h^{-1}$  kpc. We use a cell opening angle of  $\Theta < 0.8$  at low redshift, and  $\Theta < 0.7$  at  $z > 2$ . In Section 4.2, we discuss tests that confirm that our choices of initial redshift, softening, and high-redshift opening angle are adequate (see Table 1). We use a ‘multisteping’ approach, where particles in the highest density regions undergo 16 000 time-steps. Time-steps were constrained to  $\delta t < 0.2\sqrt{\epsilon/a}$ , where  $\epsilon$  is the softening length and  $a$  is the magnitude of the acceleration of a given particle. We normalize the density power spectrum of our initial conditions such that  $\sigma_8$ , the rms density fluctuation of spheres of  $8 h^{-1}$  Mpc extrapolated to redshift of zero, is 1.0, consistent with both the cluster abundance (see e.g. Eke, Cole & Frenk 1996, and references therein) and the COBE normalization (e.g. Ratra et al. 1997). To set our initial conditions, we use the Bardeen et al. (1986) transfer function with  $\gamma = \Omega_m h$ , where  $h$  is the hubble constant in units of  $100 \text{ km s}^{-1} \text{ Mpc}^{-1}$ .

### 2.1 Halo identification

In order to identify haloes in our simulation, we use both the *friends-of-friends* (FOF) algorithm (Davis et al. 1985), and the *spherical overdensity* (SO) algorithm (Lacey & Cole 1994). The FOF halo finder uses a ‘linking length’,  $l$ , to link together all neighbouring particles with spacing closer than  $l$  as members of a halo. SO identifies haloes by identifying spherical regions with the expected spherical overdensities of virialized haloes. For our SO haloes, we first use SKID (Stadel 2001) to identify all bound haloes, including those that are subhaloes within larger haloes. Next, we grow a sphere outward from each SKID centre until it just contains the virialized overdensity. Finally, we iterate by growing spheres outward from all neighbouring SKID haloes until we have identified the centre of mass for each SO halo. For our SO criterion, we use the virial overdensity predicted by the spherical collapse top-hat model of Eke et al. (1996). In a  $\Lambda$ CDM universe, the virial overdensity, in units of critical density, declines from an asymptotic value of 178 as cosmic time increases and  $\Omega_m$  drops below 1; for redshift of zero, the  $\Lambda$ CDM overdensity  $\Delta_{\text{vir}}$  is 100 (Kitayama & Suto 1996). We exclude haloes that contain less than 64 particles, which is conservative, as it is more than the estimated 20 or 30 particles needed for a robust halo identification based on resolution tests (Jenkins et al. 2001; Governato et al. 1999).

We utilize the FOF algorithm for the bulk of our analyses since it is reasonably robust and computationally efficient. Our FOF  $l$  choice is 0.2 for all redshifts (except when matching  $l$  from previous studies); this approach has been shown to be sound for a range of cosmologies by Jenkins et al. (2001), although the evolution of  $\Delta_{\text{vir}}$  in the spherical collapse top-hat model implies that  $l$  should range from  $l = 0.164$  at  $z = 0$  to  $l = 0.2$  at high redshift in  $\Lambda$ CDM cosmology (Lacey & Cole 1994; Eke et al. 1996; Jenkins et al. 2001). To test the sensitivity of the mass function to halo selection

**Table 1.**  $N$ -body simulation parameters, including test runs.

$z_0$	$r_{\text{soft}} (h^{-1} \text{ kpc})$	$\Theta(z > 7)$	$n_{\text{replica}}$	$z_{\text{evolved}}$	$\Theta(2 < z < 7)$	$\Theta(z < 2)$	
69	5.0	0.7	1	0	0.7	0.8	Applied to $z < 7$ results; SO vs. FOF test
139	5.0	0.5	1	7	–	–	Applied to $z \geq 7$ results
139	5.0	0.5	2	7	–	–	Test
69	2.5	0.7	1	7	–	–	Test
39	5.0	0.7	1	10	–	–	Test
279	5.0	0.5	2	7	–	–	Test

criteria, we apply both FOF  $ll = 0.164$  and SO to our data at various redshifts, discussed in Section 4.1.

### 3 ANALYTIC THEORY

Analytic P-S formalism yields the following (See Jenkins et al. 2001, whose notation we adopt in this section, and references therein for further discussion, which we summarize here):

$$f(\sigma; \text{P-S}) = \sqrt{\frac{2}{\pi}} \frac{\delta_c}{\sigma} \exp \left[ -\frac{\delta_c^2}{2\sigma^2} \right], \quad (1)$$

where  $\delta_c$  is the threshold spherical linear overdensity above which a region will collapse.  $\delta_c$  depends only weakly on the cosmological parameters and redshift (e.g. More, Heavens & Peacock 1986; Jenkins et al. 2001), and  $\delta_c = 1.686$  for  $\Omega_0 = 1$ . In our analysis, we assume that  $\delta_c = 1.686$  at all redshifts.  $\sigma^2(M, z)$  is the variance of the linear density field, smoothed with a spherical top-hat filter enclosing mass  $M$ , and is calculated from the linear density power spectrum  $P(k)$ , extrapolated to  $z = 0$ :

$$\sigma^2(M, z) = \frac{b^2(z)}{2\pi^2} \int_0^\infty k^2 P(k) W^2(k; M) dk, \quad (2)$$

where  $W(k; M)$  is the Fourier-space top-hat filter, and  $b(z)$  is the growth factor of linear perturbations normalized to unity at  $z = 0$  (Peebles 1993). In the P-S formalism, all mass is contained in haloes:

$$\int_{-\infty}^\infty f(\sigma; \text{P-S}) d \ln \sigma^{-1} = 1. \quad (3)$$

The mass function  $f(\sigma, z)$  can be related to the number density,  $n(M, z)$ , of haloes with mass less than  $M$ :

$$f(\sigma, z) \equiv \frac{M}{\rho_0(z)} \frac{dn(M, z)}{d \ln \sigma^{-1}}, \quad (4)$$

where  $\rho_0(z)$  is the mean density of the universe at that time.

The S-T model is a modification to the P-S model based on empirical fits to simulations (Sheth & Tormen 1999), has been shown to reproduce simulation results substantially better than P-S (e.g. Jenkins et al. 2001; White 2002), and is theoretically justified in that it matches P-S formalism derived with ellipsoidal halo collapse models (Sheth et al. 2001):

$$f(\sigma; \text{S-T}) = A \sqrt{\frac{2a}{\pi}} \left[ 1 + \left( \frac{\sigma^2}{a\delta_c^2} \right)^p \right] \frac{\delta_c}{\sigma} \exp \left[ -\frac{a\delta_c^2}{2\sigma^2} \right], \quad (5)$$

where  $A = 0.3222$ ,  $a = 0.707$  and  $p = 0.3$ . Jenkins et al. (2001) offer an empirical fit using high-resolution simulations of a range of cosmologies. Their fit is constructed in the  $f - \ln(\sigma^{-1})$  plane, which has the advantage of being invariant with redshift:

$$f(\ln \sigma^{-1}) = 0.315 \exp[-|\ln \sigma^{-1} + 0.61|^{3.8}]. \quad (6)$$

The Jenkins et al. function adjusts for an overprediction by the S-T function for the rare objects at large  $\ln \sigma^{-1}$ , and is calibrated for the range  $-1.2 \leq \ln \sigma^{-1} \leq 1.05$ , which corresponds to masses down to approximately  $3 \times 10^{11} h^{-1} M_\odot$  at present epoch, and includes haloes out to  $z = 5$ , with FOF fixed at  $ll = 0.2$ .

In each of these analytic functions, virialized haloes have a characteristic mass,  $M_*(z)$ :

$$\sigma(M_*(z)) = \delta_c, \quad (7)$$

and  $\sigma(M, z) = \sigma(M, z=0)b(z)$ .  $b(z)$  evolves as  $(1+z)^{-1}$  in an  $\Omega_0 = 1$  universe, and more slowly in a  $\Lambda$ CDM universe.  $\sigma(M)$  decreases

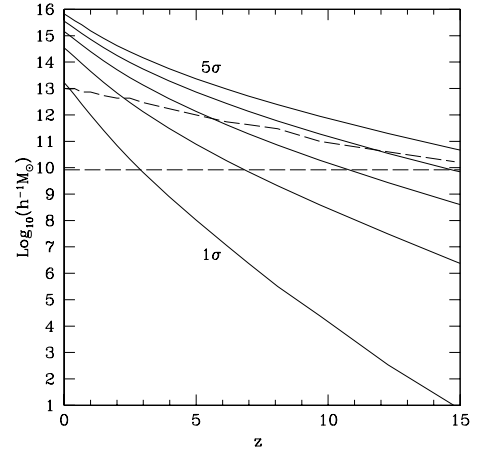


**Figure 1.** The curves correspond to the halo mass of  $n\sigma$  fluctuations in the density field, given by  $\sigma(M, z) = \delta_c/n$ , with  $n = 1, 2, 3, 4$  and  $5$ , from bottom to top. The characteristic mass,  $M_*$ , given by  $\sigma(M_*(z)) = \delta_c$ , is the  $1\sigma$  curve. The area between the long dashed lines is sampled with Poisson errors of less than 20 per cent in our data.

slowly with increasing mass, which leads to the steep redshift dependence of  $M_*(z)$ , shown in Fig. 1 for the  $\Lambda$ CDM universe, and results in a broad mass spectrum of collapsed objects. An important test of analytic mass functions is the accuracy of their predictions at high values of  $M/M_*$  and  $z$ . At low redshift, high  $M/M_*$  haloes would have unrealistically large masses, but at high redshift the steep evolution of  $M_*$  puts high  $M/M_*$  objects well into the realm of simulations. Furthermore, the evolution of halo masses that correspond to high  $\sigma$  density enhancements means that rare haloes are most easily simulated at high redshift (Fig. 1). Our simulations model the mass function of haloes lying at up to  $4\sigma$  density fluctuations.

### 4 EVOLUTION OF THE MASS FUNCTION

In Fig. 2, we compare the analytic version of the P-S, the S-T, and the Jenkins et al. mass function with our simulation results at several redshifts. The S-T function provides the best fit to our simulation with excellent agreement at all masses and redshifts except for our highest redshift outputs. The P-S function overpredicts substantially everywhere except at the low- and high-mass extremes. And the Jenkins et al. mass function fits much of our data well at  $z = 0$ , but diverges from our simulation results once well below the limit of its empirical fit of  $\ln \sigma^{-1} = -1.2$ , which corresponds to  $\simeq 4 \times 10^{11} h^{-1} M_\odot$  with  $\sigma_8 = 1.0$ . Note that  $\sigma(M, z)$  is sensitive to  $\sigma_8$ , so for a  $\sigma_8 = 0.9\Lambda$ CDM model, which was used in many of the simulations that were part of the Jenkins et al. fit,  $\ln \sigma^{-1} = -1.2$  would correspond to only  $\simeq 2 \times 10^{11} h^{-1} M_\odot$ .

In Fig. 3, we show the evolution of the mass function over all of our redshifts compared to its S-T predicted evolution. The S-T function provides an excellent fit to our data, except at very high redshifts, where it significantly overpredicts the halo abundance. At all redshifts up to  $z = 10$ , the difference is  $\lesssim 10$  per cent for each of our well-sampled mass bins. However, the S-T function begins to overpredict the number of haloes increasingly with redshift for  $z \gtrsim 10$ , up to  $\sim 50$  per cent by  $z = 15$ . The simulation mass functions appear to be generally steeper than the S-T function, especially at high redshifts. In Fig. 4, we show the evolution of the mass function over all of our redshifts as a function of  $M/M_*$ . This highlights the

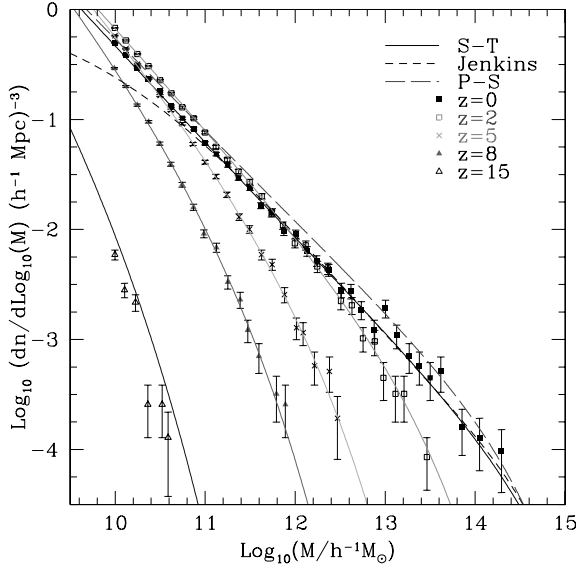


**Figure 2.** Comparison of the mass function per decade of mass. Data points are our  $\Lambda$ CDM simulation results with  $1\sigma$  Poisson error bars. Throughout the paper, haloes are identified using a FOF  $ll = 0.2$ , unless otherwise specified; only haloes with at least 64 particles are considered. In our plots, we plot the median halo mass in a bin. Solid curves are the Sheth & Tormen function at  $z = 0, 2, 5, 8$  and  $15$ . The short-dashed curve is the Jenkins et al. ‘universal’ mass function (equation 6), which diverges when extrapolated well below its original lower mass limit of  $\simeq 4 \times 10^{11} h^{-1} M_{\odot}$  for our  $\sigma_8 = 1.0$  model (see text). The long-dashed curve is the Press & Schechter function. This figure can be seen in colour in the on-line version of the journal on *Synergy*.

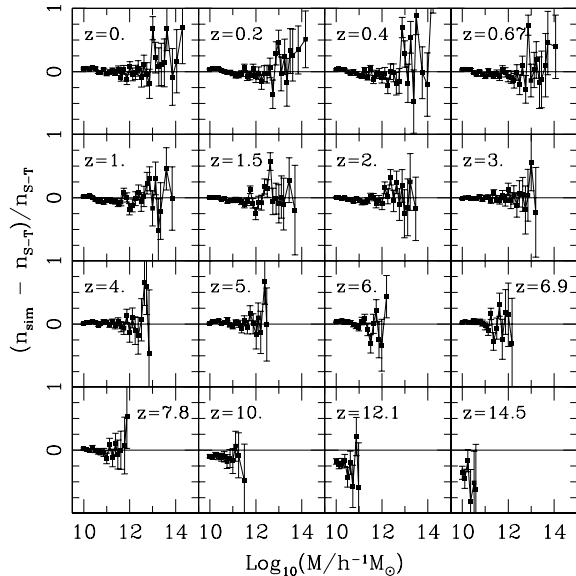


**Figure 3.** Fractional difference between our simulated mass function (FOF  $ll = 0.2$ ) and the S-T prediction. Poisson error bars shown.

remarkable accuracy of the S-T mass function over more than 10 decades of  $M/M_*$ .

In Fig. 5, we plot the mass function for all of our outputs in the  $f - \ln(\sigma^{-1})$  plane. Large values of  $\ln \sigma^{-1}$  correspond to rare haloes of high redshift and/or high mass, while small values of  $\ln \sigma^{-1}$  describe haloes of low mass and redshift combinations. In Fig. 6, we compare our simulated mass function with the S-T prediction, by plotting the residuals over our entire range. We limit plotted data to

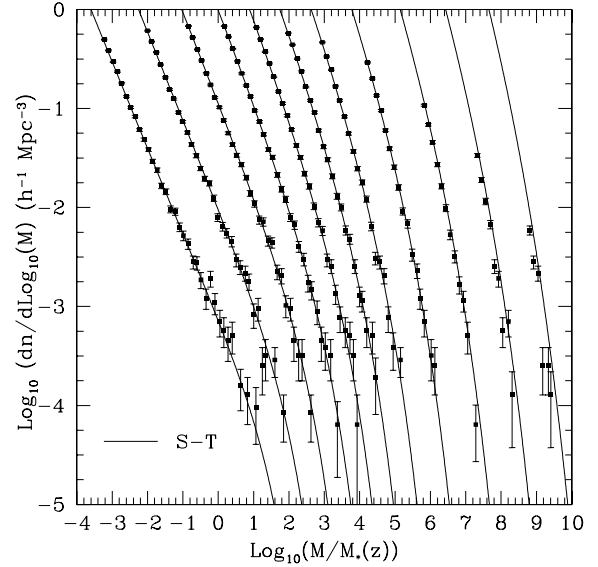


**Figure 4.** Number density versus  $M/M_*$ . Data points with Poisson error bars are our simulation results. Curves are S-T predictions. Redshifts plotted are (from left to right) 0, 1, 2, 3, 4, 5, 6.2, 7.8, 10, 12.1, 14.5.

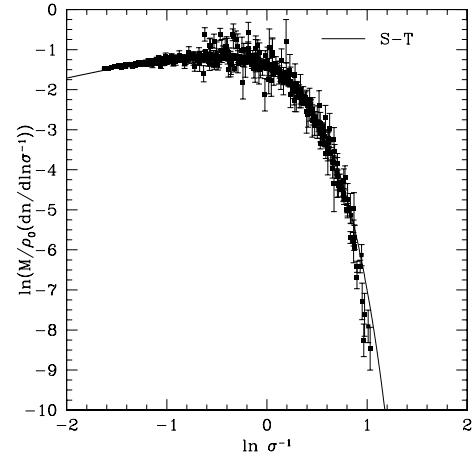


**Figure 5.** Mass function plotted in redshift independent form for all of our outputs as in Fig. 4. Solid curve is the S-T prediction.

bins with Poisson errors of less than 20 per cent. Remarkably, the S-T function fits our simulated mass function to better than 10 per cent over the range of  $-1.7 \leq \ln \sigma^{-1} \leq 0.5$ . We are unaware of any previous studies that probe the mass function down to such low values of  $\ln \sigma^{-1}$  in a cosmological environment. The S-T function appears to significantly overpredict haloes for  $\ln \sigma^{-1} \geq 0.5$ . This is the same overprediction seen in the number density for  $z \geq 10$  in Figs 3 and 4. The large apparent scatter of the mass function for  $\ln \sigma^{-1} \gtrsim 0.5$  is the result of larger Poisson errors in this range. For large  $\ln \sigma^{-1}$ , we estimate the uncertainty in the mass function arising from cosmic variance by estimating the contribution of linear fluctuations on the scale of the box size. Cosmic variance can have large effects on results since it has the potential to increase or decrease the mass function in multiple mass bins simultaneously, and cosmic variance is difficult to quantify without a large set of simulated volumes. In our estimation, we use a second-order Taylor expansion of  $f(\sigma; S-T)$ , ignoring the first-order term since we have imposed the average

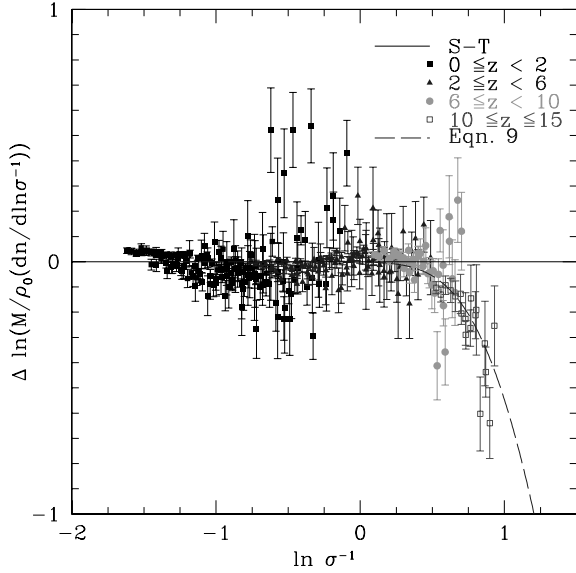


**Figure 6.** Residuals between S-T prediction and our results for the mass function of Fig. 5 (with FOF  $l = 0.2$ ). Solid straight line is the S-T function. Dashed line is our empirical adjustment to the S-T function. This figure can be seen in colour in the on-line version of the journal on *Synergy*.

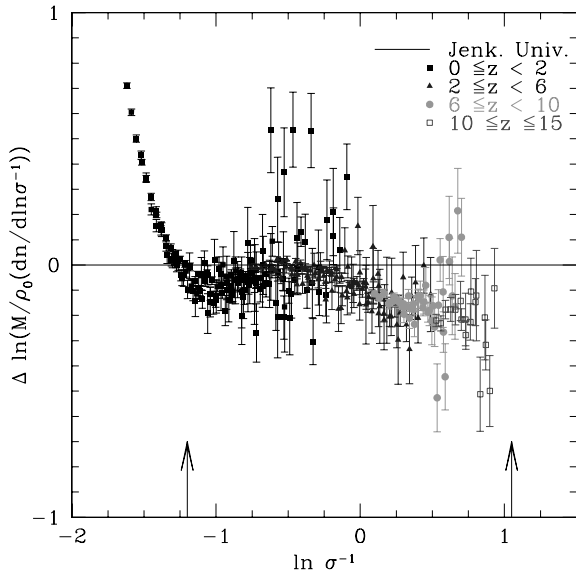


**Figure 7.** Residuals between Jenkins et al. mass function and our results for the mass function of Fig. 5. Arrows encompass the range of data used in the Jenkins et al. empirical fit, which is denoted by the solid straight line. This figure can be seen in colour in the on-line version of the journal on *Synergy*.

density of our simulation to be  $\Omega_m$ . The resulting estimate for the uncertainty in the mass function arising from cosmic variance is

$$\Delta_{f,c.v.} \sim \frac{\partial^2 f(\sigma; S-T)}{\partial \sigma^2} \frac{1}{2} \sigma_{\text{Mbox}}^2,$$

which we evaluate numerically. In our well-sampled, low-redshift mass bins,  $\Delta_{f,c.v.}$  is negligible. For our highest redshift results,  $\Delta_{f,c.v.}$  is smaller than our Poisson error limit of 20 per cent for Figs 6 and 7, even for our highest mass bins. However,  $\Delta_{f,c.v.}$  approaches our Poisson error limit of 20 per cent for our  $z = 14.5$  output. For our  $z = 10$  and  $z = 12$  outputs,  $\Delta_{f,c.v.}$  is less than 10 per cent in bins where Poisson errors are less than 10 per cent, which is the case for most of

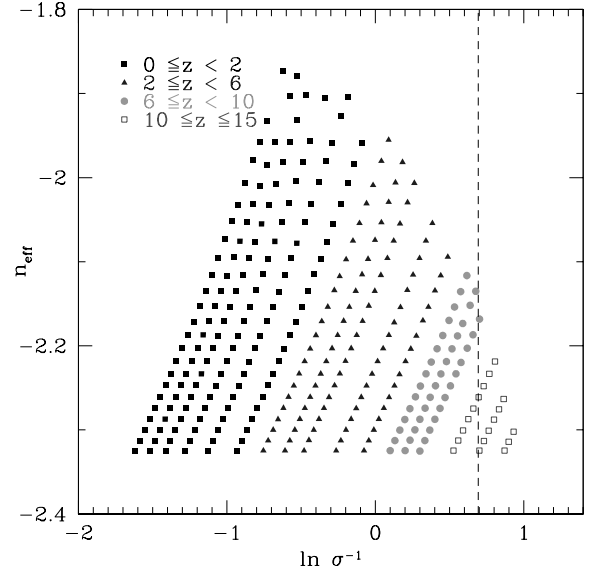


**Figure 8.** Parameter range covered by our results. Each mass bin for which we have Poisson statistics of better than 20 per cent error is shown. The vertical line denotes  $\sigma = 0.5$ . This figure can be seen in colour in the on-line version of the journal on *Synergy*.

our bins at that redshift. Thus, while cosmic variance is a significant source of error where the mass function is steepest, it is unlikely to entirely account for our discrepancy with the S-T function. We note that several of our  $z < 2$  points lie roughly  $3\sigma$  above the mean; this is actually just one mass bin plotted repeatedly at different redshifts, and so is not entirely surprising. By careful examination of ranges of  $\ln \sigma^{-1}$  where outputs of different redshifts overlap, we verify that the magnitude of the S-T overprediction at high values of  $\ln \sigma^{-1}$  is consistent with being a function purely of  $\ln \sigma^{-1}$  rather than redshift, a natural consequence of the fact that the mass function is self similar in time (e.g. Efstathiou et al. 1988; Lacey & Cole 1994; Jenkins et al. 2001). Jenkins et al. (2001) also find an overprediction by the S-T function for  $\ln \sigma^{-1} \gtrsim 0.75$ , which with their larger simulation volumes, corresponded primarily to objects of  $z \leq 2$  and of much higher mass. Additionally, Jenkins et al. find the mass function to be invariant with redshift within their own results. In Fig. 7, we compare a subset of our data with the Jenkins et al. ‘universal’ mass function. We note that when extrapolated to  $\ln \sigma^{-1} \leq -1.4$ , well below its empirical fit range of  $-1.2 \leq \ln \sigma^{-1} \leq 1.05$ , the Jenkins et al. function diverges from our results, reflecting the fact that it is of a form not ideally suited for extrapolation. Where our data overlap ( $\ln \sigma^{-1} \gtrsim -1.2$ ), we find generally good agreement, although we have  $\sim 20$  per cent fewer haloes and a somewhat steeper mass function at  $\ln \sigma^{-1} \gtrsim 0.25$ . Over the range of  $-1.4 \lesssim \ln \sigma^{-1} \gtrsim 0.75$ , the Jenkins et al. mass function matches our data to within  $\sim 20$  per cent.

We consider the possibility that this difference between our data and the Jenkins et al. fit could be the result of differences in the effective slope of the power spectrum,  $n_{\text{eff}}$ , where  $P(k) \propto k^{n_{\text{eff}}}$ . Applying a simple power law to equation (2) yields  $\sigma^2 \propto M^{-(n_{\text{eff}}+3)/3}$ , which can be reparametrized as

$$n_{\text{eff}} = 6 \frac{d \ln \sigma^{-1}}{d \ln M} - 3, \quad (8)$$

(Jenkins et al. 2001). Fig. 8 shows the  $n_{\text{eff}}$  versus  $\ln \sigma^{-1}$  parameter space that our results cover. Our data generally has a steeper  $n_{\text{eff}}$  than Jenkins et al., though there is some overlap, especially at lower

redshifts. Since the slope of the linear power spectrum is invariant with redshift for a given  $k$ ,  $n_{\text{eff}}(z)$  is constant for a given mass, meaning that for our lowest mass haloes we sample nearly all of our  $f(\sigma)$  at an  $n_{\text{eff}} \simeq -2.3$ . If we consider  $n_{\text{eff}}(\sigma = 0.5)$ , where the power spectrum begins to go non-linear, then we find that our results differ significantly from the Jenkins et al. function only where  $n_{\text{eff}}$  at the non-linear scale is steepest. In particular, the disagreement is worst at  $z \geq 10$  where  $n_{\text{eff}}(\sigma = 0.5)$  exceeds their maximum value of  $-2.26$ . Thus, there is a possibility that our steeper values of  $n_{\text{eff}}$  results in an  $f(\sigma)$  with a slightly different shape, which might account for the difference with prior results, but a larger set of simulations with still steeper  $n_{\text{eff}}$  would be needed to clearly show any such dependence.

Since no mass function that we have considered is accurate for the entire range of our data, we consider the possibility of an empirical adjustment to the S-T function. We insert a crude multiplicative factor to the S-T function as follows, with  $\delta_c = 1.686$  and FOF  $ll = 0.2$  (Fig. 6):

$$f(\sigma) = f(\sigma; \text{S-T}) \{ \exp[-0.7/(\sigma [\cosh(2\sigma)]^5)] \}, \quad (9)$$

valid over the range of  $-1.7 \leq \ln \sigma^{-1} \leq 0.9$ . The resulting function is virtually identical to the S-T function for all  $-\infty \leq \ln \sigma \leq 0.4$ . At higher values of  $\ln \sigma^{-1}$ , this function declines relative to the S-T function, reflecting an underabundance of haloes that becomes greater with increasing  $\ln \sigma^{-1}$ . For  $-1.7 \leq \ln \sigma^{-1} \leq 0.5$ , equation (9) matches our data to better than 10 per cent for well-sampled bins, while for  $0.5 \leq \ln \sigma^{-1} \leq 0.9$ , where Poisson errors are larger, our data is matched to roughly 20 per cent. We must caution that though equation (9) is a good fit to our data, it differs from the S-T function in the regime where Poisson and cosmic errors are highest, and where our results are most prone to potential numerical errors because of the steepness of the mass function. Our results are more robust in the low  $\ln \sigma^{-1}$  regime. Note that in the equation (9) fit, not all mass belongs to a halo, so equation (3) is not valid.

#### 4.1 Friends-of-friends (FOF) versus spherical overdensity (SO)

Other authors have noted the advantages and disadvantages of the FOF and SO algorithms (see Jenkins et al. 2001, and references therein). The FOF method has the advantage that it can identify haloes of any shape as long as their minimum local number density is at least roughly  $1/b^3$ , and FOF is generally computationally cheaper than SO. However, FOF can sometimes spuriously link together haloes that lie close together within a filament (see e.g. Governato et al. 1997). In Fig. 9, we compare FOF mass functions of our simulation with the corresponding SO mass functions for a range of redshifts. Note that the vertical axes are somewhat arbitrary for the  $z = 10$  and  $z = 15$  outputs as these were made from the  $z_0 = 69$  version of the simulation which had a somewhat suppressed mass function, which we discuss in Section 4.2. The halo finders have excellent agreement at low redshifts, with differences of  $\lesssim 10$  per cent over the range where the mass function is well sampled. Differences in the high mass bins are due to a combination of different mass calculations for individual selected clusters as well as offset mass bins. The steep drop-off in the SO mass function for low masses is due to our exclusion of SKID haloes of less than 64 particles as potential SO centres. At high redshifts, FOF  $ll = 0.2$  produces a substantially higher mass function than FOF  $ll = 0.164$  or SO, which are similar to each other, implying sensitivity to  $ll$  for large  $\ln \sigma^{-1}$ , probably because the mass function is steep there, and thus sensitive to halo selection criteria. To verify that the discrepancy of FOF  $ll = 0.2$  with SO is not due simply to our choice

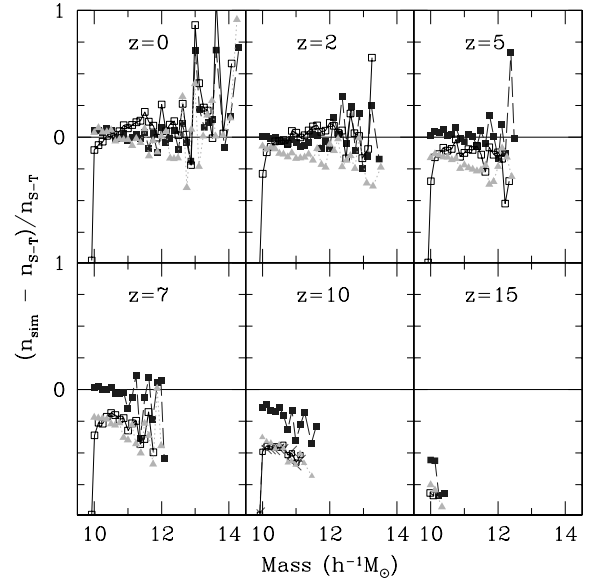


**Figure 9.** Comparison of SO and FOF mass functions from our simulation. Filled squares (connected by dashed lines) are for FOF  $ll = 0.2$  haloes; filled triangles (connected by dotted lines) are FOF  $ll = 0.164$  haloes. Open squares (solid lines) are SO haloes made with SKID centres. X's at  $z = 10$  are SO haloes made using FOF centres. The SO overdensity criterion is from Kitayama & Suto (1996). Note that the  $z = 10$  and  $z = 15$  data lie too far below the S-T function in this plot because it is from our  $z_0 = 69$  run rather than our  $z_0 = 139$  run, which we use for the rest of the high-redshift results of this paper. This figure can be seen in colour in the on-line version of the journal on *Synergy*.

of using skid haloes as our initial SO centres, we have included a high-redshift ( $z = 10$ ) SO mass function which uses FOF haloes as initial SO centres; our choice of centres from which to grow our SO spheres has no effect on the SO mass function. A visual inspection in which halo members are ‘marked’ reveals that at high redshift, FOF  $ll = 0.2$  links together some neighbouring haloes connected by filaments, but FOF also identifies some individual haloes (often of highly elongated shape) that are missed by SO, so neither algorithm is ideal. The overprediction of the S-T function for rare objects worsens somewhat if we use SO derived mass functions. Using a linking length that varies with redshift in an attempt to match the varying overdensity of virialized haloes, would have little effect on our mass function, since at low redshift the mass function is insensitive to  $ll$ , and at high redshift  $\Omega_m \simeq 1$ , implying  $ll = 0.2$  (Davis et al. 1985; Lacey & Cole 1994). However, had we sampled large  $\ln \sigma^{-1}$  at low redshift, adjusting  $ll$  to match virial overdensity would likely have a significant effect.

#### 4.2 Numerical tests

We check that the disagreement of S-T which appears at high redshift is not a result of delayed halo collapse arising from numerical errors, which can be caused by too large of a gravitational softening length. We make additional checks addressing potential numerical errors caused by mapping particles with Zel’dovich displacements (Zel’dovich 1970) on to a particle grid; an insufficiently high starting redshift could delay collapse of the first haloes (e.g. Jenkins et al. 2001). If initial conditions are set with some regions having overdensities high enough to already be in the non-linear regime, then the linear Zel’dovich mapping can not account for shell-crossing wherein mass piles up as it flows toward overdensities. The effects of either of these error sources, if present, should have evolved away

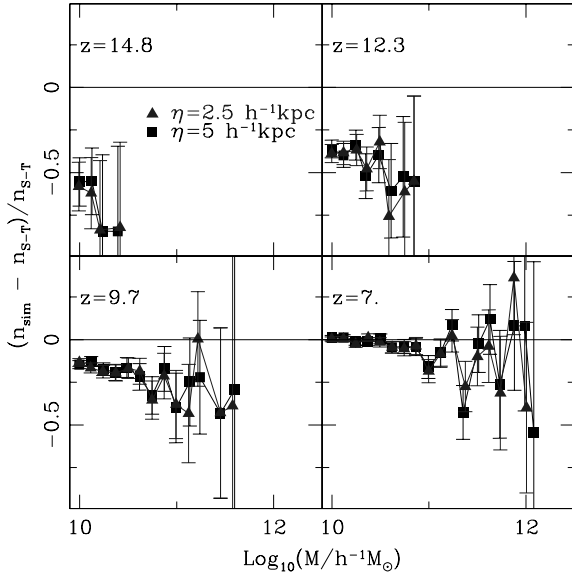


**Figure 10.** The high-redshift mass functions for runs with softening lengths of  $5 h^{-1}$  kpc and  $2.5 h^{-1}$  kpc. Both runs were started from a redshift of 69. This figure can be seen in colour in the on-line version of the journal on *Synergy*.

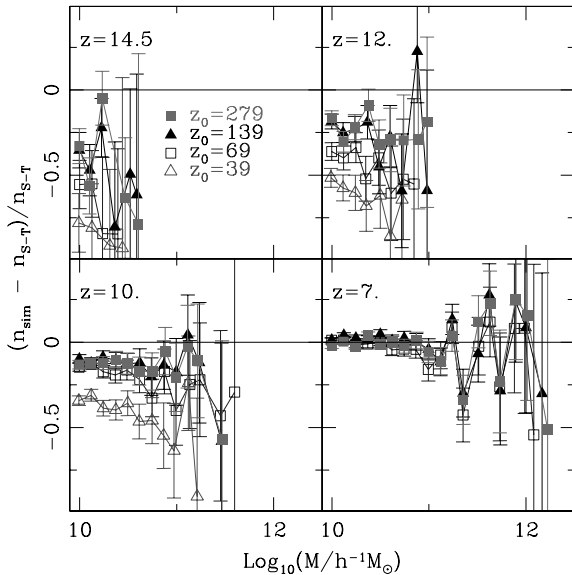


**Figure 11.** The high-redshift mass functions for initial redshifts of 39, 69, 139, and 279. Each run has a softening of  $5 h^{-1}$  kpc. The  $z_0 = 39$  run was stopped at  $z = 10$ . This figure can be seen in colour in the on-line version of the journal on *Synergy*.

by lower redshifts, since the tiny fraction of matter that is in haloes at such high redshifts is soon incorporated into clusters or large groups.

Table 1 lists our test runs, each of which consists of an identical  $432^3$  particle volume with identical random waves, and is evolved to  $z = 7$ . Fig. 10 shows the mass function for  $z \simeq 7-15$  for our low softening test run, started from  $z_0 = 69$ , and plotted relative to the S-T function along with our  $z_0 = 69$ ,  $5 h^{-1}$  kpc data. Halving the softening to  $2.5 h^{-1}$  kpc has no effect on the mass function. Fig. 11 shows the mass function for  $z \simeq 7-15$  for our initial redshift test runs, all with  $5 h^{-1}$  kpc softening. Lowering the initial redshift to 39 substantially reduces the number of high-redshift haloes, so we

did not evolve the  $z_0 = 39$  run to  $z < 10$ . The  $z_0 = 139$  run matches the  $z_0 = 279$  run, indicating convergence, but the  $z_0 = 69$  run has a reduced mass function relative to the  $z_0 = 139$  run at redshifts  $z \gtrsim 12$ . By  $z = 7$ , however, the  $z_0 = 139$  and  $z_0 = 69$  mass functions have converged, showing that evolving the simulation over an expansion factor of  $\simeq 10$  from initial conditions is sufficient for mass function measurements. We consequently derive our low-redshift ( $z < 7$ ) results throughout this paper from the  $z_0 = 69$ ,  $5 h^{-1}$  kpc simulation, and utilize the  $z_0 = 139$  run for our  $z \geq 7$  results. We make an additional test of  $z \geq 7$  cell opening angle, which is used to determine how accurately long range gravitational forces are to be approximated. If the cell opening angle is too large, then artificial net forces will be incurred upon particles, which could cause ‘spurious’ haloes to form. This effect is most likely to occur at high redshifts when gravitational perturbations are small and force errors are fractionally larger. Decreasing the opening angle from  $\Theta = 0.7$  to  $\Theta = 0.5$ , for our  $z_0 = 139$  case, had no appreciable effect on the mass function for  $z \geq 7$ . We test that the number of replicas used for our periodic boundaries,  $n_r = 1$ , is adequate. With  $z_0 = 139$ , increasing  $n_r$  from 1 to 2 has no effect on the mass function. Additionally, to test that our box size is adequate, we have verified that our  $z = 0$  mass function agrees with the mass function from larger, lower resolution volumes where they overlap (not included in Table 1).

## 5 CONCLUSIONS

Our results extend to lower masses and higher redshifts than the original empirical fit of the S-T mass function. The range of masses and redshifts over which the S-T mass function remains valid is quite remarkable, and though it does begin to break down at redshift  $\gtrsim 10$  in our results, no other function matches its range and accuracy. It is not well understood why the mass function can be described so well by solely  $\sigma(M)$ . Lacey & Cole (1994), in simulations with scale-free power spectra, found evidence that the mass function depends on  $n_{\text{eff}}$  as well as  $\sigma$ , though they tested a wider range in  $n_{\text{eff}}$  than in more recent CDM simulations. The generally good agreement of our data with previous work at much shallower  $n_{\text{eff}}$  implies that any such dependence is weak, though it may be manifested in our results where we differ from the S-T function. As  $n_{\text{eff}}$  approaches  $-3$ , the growth of  $M_*$  with time diverges, so any dependence of  $f(\sigma)$  on  $n_{\text{eff}}$  is most likely to occur near that regime. Simulations with finer mass resolution will be able to test yet steeper values of  $n_{\text{eff}}$ . Based on the apparent trend of the S-T function to overpredict halo numbers for objects of greater rarity, we expect that the overprediction of the S-T function may continue to worsen when even higher values of  $\ln \sigma^{-1}$ , or equivalently, when more extreme values of  $M/M_*$  and redshift, are analysed. Theoretical work that focuses on halo collapse in this high  $\ln \sigma^{-1}$  range is needed to produce more robust predictions.

Because the form of the mass function for low-mass, low-redshift haloes closely resembles a power law, we are cautiously optimistic that the S-T mass function will continue to provide a good match to simulation data as lower values of  $\ln \sigma^{-1}$  are modelled, though this extrapolation will likely breakdown where  $n_{\text{eff}}$  approaches  $-3$ . Simulations that model higher particle numbers (leading to higher redshifts), are needed to extend the known range of the mass function of dark matter haloes. The accuracy of the S-T function for low-mass haloes out to high redshifts has important implications for a number of astrophysical problems. Evolution of the mass and luminosity functions down to dwarf scales permits comparison with surveys, providing important cosmological tests, and allows calculations of merger histories and star formation histories of galaxies, groups,

and clusters. Our results verify that the S–T function is accurate over the entire evolutionary range (for which progenitors or descendants are observable) of Lyman-break galaxies and groups of galaxies. Assuming a weak dependence on  $n_{\text{eff}}$ , the redshift invariance of the mass function implies that extrapolation of mass functions should be reliable for combinations of masses and redshifts that cannot presently be simulated, as long as only values of  $\ln \sigma^{-1}$  that have been verified by simulation are considered. The number densities of low-mass ( $<10^{10} M_{\odot}$ ) haloes at high redshift ( $z \sim 10$ ), needed for studies of reionization, or galaxy formation (e.g. Haiman 2003), should be well described by the S–T function since although they lie below our mass range, they are within our range of simulated  $\ln \sigma^{-1}$ . For such extrapolation to be accurate down to indefinitely small masses, all mass would have to be in dark matter haloes of some mass or else low-mass haloes would be overpredicted.

Extrapolation of mass functions to large values of  $\ln \sigma^{-1}$  that have yet to be verified by simulations, however, are likely to be significantly in error, as suggested by the trend of increasing overprediction by the S–T function for high values of  $\ln \sigma^{-1}$ . Though our results only reach  $\simeq 4\sigma$  density peaks, there is a trend for the S–T function to increasingly overpredict the mass function for increasing  $\sigma$  beginning at  $\simeq 3\sigma$ . The discrepancy with the S–T function for rare objects has significant implications for studies that make use of such rare objects as a cosmological probe. For example, the number density of high-redshift ( $z \simeq 6$ ) QSOs, which are thought to be hosted by haloes at  $5\sigma$  peaks in the fluctuation field (Haiman & Loeb 2001; Fan et al. 2001), are likely to be overpredicted by at least a factor of 50 per cent. Some uncertainty is also introduced for studies employing the abundance of the highest redshift clusters to probe cosmological parameters (e.g. Robinson, Gawiser & Silk 2000, and references therein).

### 5.1 Summary

In summary, we have utilized high-resolution simulations to derive the mass function of dark matter haloes over an extended range in both mass and redshift over previous work. We find that the S–T mass function holds up exceptionally over more than 10 orders of magnitude of  $M/M_*$ . For  $-1.7 \leq \ln \sigma^{-1} \leq 0.5$ , the S–T mass function is an excellent fit to our data, but begins to overpredict haloes for  $\ln(\sigma^{-1}) \gtrsim 0.5$ , or  $M/M_* \gtrsim 10^6$  in our volume, reaching a  $\sim 50$  per cent discrepancy by  $\ln(\sigma^{-1}) \simeq 0.9$ , corresponding to  $M/M_* \sim 10^9$  at  $z \simeq 15$  in our volume. We offer an empirical adjustment for the high  $\ln(\sigma^{-1})$  portion of the S–T mass function. Our results confirm the redshift invariance of the mass function.

### ACKNOWLEDGMENTS

We graciously thank the referee, Adrian Jenkins, for extremely helpful suggestions for improvements to this paper. This work was supported, in part by NASA training grant NGT5-126. Our simulations were performed on the Origin 2000 at NCSA and NASA Ames, the IBM SP4 at the Arctic Region Supercomputing Centre (ARSC), and the NASA Goddard HP/Compaq SC 45. We thank Chance Reschke

for dedicated support of our computing resources, much of which were graciously donated by Intel.

### REFERENCES

- Bardeen J. M., Bond J. R., Kaiser N., Szalay A. S., 1986, *ApJ*, 305, 15  
 Bond J. R., Cole S., Efstathiou G., Kaiser N., 1991, *ApJ*, 379, 440  
 Bower R. G., 1991, *MNRAS*, 248, 332  
 Davis M., Efstathiou G., Frenk C. S., White S. D. M., 1985, *ApJ*, 292, 381  
 Efstathiou G., Frenk C. S., White S. D. M., Davis M., 1988, *MNRAS*, 235, 715  
 Eke V. R., Cole S., Frenk C. S., 1996, *MNRAS*, 282, 263  
 Evrard A. et al., 2002, *ApJ*, 573, 7  
 Fan X. et al., 2001, *AJ*, 122, 2833  
 Gardner J. P., 2001, *ApJ*, 557, 616  
 Governato F., Moore B., Cen R., Stadel J., Lake G., Quinn T., 1997, *New Astron.*, 2, 91  
 Governato F., Baugh C., Frenk C., Cole S., Lacey C., Quinn T., Stadel J., 1998, *Nat*, 392, 359  
 Governato F., Babul A., Quinn T., Tozzi P., Baugh C. M., Katz N., Lake G., 1999, *MNRAS*, 307, 949  
 Governato F., Ghigna S., Moore B., Quinn T., Stadel J., Lake G., 2001, *ApJ*, 547, 555  
 Gross M. A., Somerville R. S., Primack J. R., Holtzman J., Klypin A., 1998, *MNRAS*, 301, 81  
 Haiman Z., 2003, in Renzini A., Bender R. eds, *Proc. ESO Workshop, The Mass of Galaxies at Low and High Redshift*. Springer-Verlag, Heidelberg, p. 316  
 Haiman Z., Loeb A., 2001, *ApJ*, 552, 459  
 Jenkins A. et al., 1998, *ApJ*, 499, 20  
 Jenkins A., Frenk C. S., White S. D. M., Colberg J. M., Cole S., Evrard A. E., Couchman H. M. P., Yoshida N., 2001, *MNRAS*, 321, 372  
 Kitayama T., Suto Y., 1996, *MNRAS*, 269, 480  
 Lacey C., Cole S., 1993, *MNRAS*, 262, 627  
 Lacey C., Cole S., 1994, *MNRAS*, 271, 676  
 Lee J., Shandarin S. F., 1998, *ApJ*, 500, 14  
 Monaco P., 1997a, *MNRAS*, 287, 753  
 Monaco P., 1997b, *MNRAS*, 290, 439  
 Monaco P., Theuns T., Taffoni G., Governato F., Quinn T., Stadel J., 2002, *ApJ*, 564, 8  
 More J., Heavens A., Peacock J., 1986, *MNRAS*, 220, 189  
 Nagashima M., 2001, *ApJ*, 562, 7  
 Peebles P. J. E., 1993, *Principles of Physical Cosmology*. Princeton Univ. Press, Princeton NJ  
 Press W. H., Schechter P., 1974, *ApJ*, 187, 425  
 Ratna B., Sugiyama N., Banday A. J., Gorski K. M., 1997, *ApJ*, 481, 22  
 Robinson J., Gawiser E., Silk J., 2000, *ApJ*, 532, 1; 1997, *ApJ*, 481, 22  
 Sheth R. K., Tormen G., 1999, *MNRAS*, 308, 119  
 Sheth R. K., Mo H., Tormen G., 2001, *MNRAS*, 323, 1  
 Stadel J., 2001, PhD thesis, Univ. Washington  
 Steidel C. C., Giallisco M., Pettini M., Dickinson M., Adelberger K., 1996, *ApJ*, 162, L17  
 White M., 2002, *ApJS*, 143, 241  
 Williams R. et al., 1996, *AJ*, 112, 1335  
 Yano T., Nagashima M., Gouda N., 1996, *ApJ*, 466, 1  
 Zel'dovich YA. B., 1970, *Astrofiz.*, 6, 319 (translated in *Astrophys.*, 6, 164 [1973])

This paper has been typeset from a  $\text{\LaTeX}$  file prepared by the author.